THE JOURNAL OF BIOLOGICAL CHEMISTRY VOL. 286, NO. 4, pp. 2433–2444, January 28, 2011

Caveolin-3 Regulates Protein Kinase A Modulation of the $Ca_V3.2$ (α_{1H}) T-type Ca^{2+} Channels*[S]

Received for publication, September 7, 2010, and in revised form, October 15, 2010 Published, JBC Papers in Press, November 17, 2010, DOI 10.1074/jbc.M110.182550

Yogananda S. Markandeya[‡], Jonathan M. Fahey[‡], Florentina Pluteanu[§], Leanne L. Cribbs[§], and Ravi C. Balijepalli[‡1]

From the [‡]Department of Medicine, Cellular and Molecular Arrhythmia Research Program, University of Wisconsin, Madison, Wisconsin 53706 and the [§]Cardiovascular Institute, Loyola University Medical Center, Maywood, Illinois 60153

Voltage-gated T-type Ca^{2+} channel $Ca_v3.2$ (α_{1H}) subunit, responsible for T-type Ca^{2+} current, is expressed in different tissues and participates in Ca^{2+} entry, hormonal secretion, pacemaker activity, and arrhythmia. The precise subcellular localization and regulation of $Ca_v3.2$ channels in native cells is unknown. Caveolae containing scaffolding protein caveolin-3 (Cav-3) localize many ion channels, signaling proteins and provide temporal and spatial regulation of intracellular Ca^{2+} in different cells. We examined the localization and regulation of the $Ca_v3.2$ channels in cardiomyocytes. Immunogold labeling and electron microscopy analysis demonstrated co-localization of the $Ca_v3.2$ channel and Cav-3 relative to caveolae in ventricular myocytes. Co-immunoprecipitation from neonatal ventricular myocytes or transiently transfected HEK293 cells demonstrated that $Ca_v3.1$ and $Ca_v3.2$ channels co-immunoprecipitate with Cav-3. GST pulldown analysis confirmed that the N terminus region of Cav-3 closely interacts with $Ca_v3.2$ channels. Whole cell patch clamp analysis demonstrated that co-expression of Cav-3 significantly decreased the peak $Ca_v3.2$ current density in HEK293 cells, whereas co-expression of Cav-3 did not alter peak $Ca_v3.1$ current density. In neonatal mouse ventricular myocytes, overexpression of Cav-3 inhibited the peak T-type calcium current ($I_{Ca,T}$) and adenovirus ($AdCa_v3.2$)-mediated increase in peak $Ca_v3.2$ current, but did not affect the L-type current. The protein kinase A-dependent stimulation of $I_{Ca,T}$ by 8-Br-cAMP (membrane permeable cAMP analog) was abolished by siRNA directed against Cav-3. Our findings on functional modulation of the $Ca_v3.2$ channels by Cav-3 is important for understanding the compartmentalized regulation of Ca^{2+} signaling during normal and pathological processes.

T-type Ca^{2+} channels (TTCC)[2] are low voltage-activated Ca^{2+} channels, expressed in various tissues including brain and heart and contribute to a variety of physiological functions such as neuronal excitability, hormone secretion, muscle contraction, and pacemaker activity (1–3). Molecular cloning studies have identified three different TTCC isoforms, $Ca_V3.1$ (α_{1G}), $Ca_V3.2$ (α_{1H}), and $Ca_v3.3$ (α_{1I}), which functionally can be distinguished by their electrophysiological properties (4–7). $Ca_v3.1$ and $Ca_v3.2$ are the most commonly expressed subunits generating T-type Ca^{2+} current ($I_{Ca,T}$) in brain and heart. $Ca_v3.2$ T-type Ca^{2+} channels are involved in neurological disorders such as epilepsy and pain (8). In the heart, the $I_{Ca,T}$ participates in Ca^{2+} entry and Ca^{2+}-dependent hormonal secretion, pacemaker activity, and arrhythmia (9, 10). The $Ca_v3.1$ and $Ca_v3.2$ isoforms are normally expressed in embryonic hearts (11, 12), but postnatal expression of these isoforms diminishes with almost no expression in normal adult ventricular myocytes. However, the TTCCs are re-expressed during conditions of cardiac hypertrophy and heart failure and are reported to be associated with decreased cardiac function (13–15). Ca^{2+} influx through the re-expressed voltage-gated $Ca_v3.2$ (α_{1H}) TTCC is indicated to be responsible for inducing pathological cardiac hypertrophy in a pressure overload model (16).

Although we are beginning to understand the physiological role of $Ca_v3.2$ channels in Ca^{2+} cycling, the precise regulation of these channels has not been defined. To clearly understand the regulation and physiological function of these proteins in normal and diseased stages it is important to define the exact subcellular localization of this protein. Caveolae are specialized membrane microdomains enriched in cholesterol and sphingolipids, contain the signature scaffolding protein caveolins, and provide temporal and spatial regulation of intracellular Ca^{2+} in many cell types (17–19). Three different caveolin isoforms are identified, of which Cav-1 and Cav-2 are ubiquitously expressed (20, 21), whereas Cav-3 is widely expressed in muscle (cardiac, skeletal, and smooth muscle) cells (22) and neuronal tissue (23). A number of ion channels and transporters have been localized to caveolae and associate with Cav-3, including L-type Ca^{2+} channels ($Ca_v1.2$) (24), the Na^+ channel ($Na_v1.5$) (25), pacemaker channels (HCN4) (26), Na^+/Ca^{2+} exchanger (27), and others (18). Closely associated with these channels are specific macromolecular signaling complexes containing a variety of regulatory proteins including the G protein-coupled receptors and kinases such as PKC and PKA that provide highly localized regulation of the channels (18). The present study therefore was designed to determine the precise subcellular localization and regulation of the $Ca_v3.2$ subunit of the T-type Ca^{2+} channels. Our results dem-

* This work was supported by Scientist Development Grant 0730010N from the American Heart Association (to R. C. B.).

[S] The on-line version of this article (available at http://www.jbc.org) contains supplemental Table S1 and Figs. S1 and S2.

[1] To whom correspondence should be addressed: University of Wisconsin School of Medicine and Public Health, B370, 1300 University Ave., Madison, WI 53706. Tel.: 608-263-4066; Fax: 608-263-1144; E-mail: rcb@medicine.wisc.edu.

[2] The abbreviations used are: TTCC, voltage-gated T-type Ca^{2+} channel; Cav-3, caveolin-3; $AdCa_v3.2$, adenovirus expressing $Ca_v3.2$ channel protein; AdGFP, adenovirus expressing green fluorescent protein; TAC, transthoracic aortic constriction; PKA, cAMP-dependent protein kinase A; HCN4, hyperpolarization activated cyclic nucleotide-gated potassium channel 4; $I_{Ca,T}$, T-type calcium currents; $I_{Cav3.1}$, $Ca_v3.1$ channel calcium currents; $I_{Cav3.2}$, $Ca_v3.2$ channel calcium currents; 8-Br-CAMP, 8-bromo-cyclic AMP.

onstrate that the $Ca_v3.2$ channel protein is localized to caveolar microdomains in the ventricular myocytes and Cav-3 interacts with $Ca_v3.2$ channel and regulates its function.

EXPERIMENTAL PROCEDURES

Materials—All chemicals and reagents were procured from Sigma unless otherwise stated. Mouse monoclonal antibodies to Cav-3, cardiac actin, and biotin were obtained from BD Biosciences; rabbit polyclonal antibody to Cav-3 and control IgG antibodies were from Santa Cruz Biotechnology. Rabbit polyclonal antibodies to $Ca_v3.1$ and $Ca_v3.2$ channel were from Alamone Labs, Jerusalem, Israel; rabbit polyclonal antibody to $Ca_v3.1$ was from Millipore. Tetradotoxin was obtained from Calbiochem. PKA inhibitor peptide 14-22, myristoylated (amino acid sequence: Myr-Gly-Arg-Thr-Gly-Arg-Arg-Asn-Ala-Ile-NH_2), was from Sigma.

Cell Culture and Transfection—Wild-type human $Ca_v3.1$, $Ca_v3.2$ channels, or Cav-3 protein were expressed in human embryonic kidney 293 (HEK293) cells as previously described (28). The HEK293 cells were maintained in modified DMEM (Invitrogen) and cultured at 37 °C in 5% CO_2. HEK293 cells were transfected using Lipofectamine 2000 (Invitrogen) as described previously (29). 48 h after transient transfection the cells were used for experiments. Neonatal or adult mouse ventricular myocytes were enzymatically isolated as previously described (24, 30). The neonatal myocytes were transfected by the electroporation method by a Nucleofector device (AMAXA) as described earlier (24) using Ingenio electroporation reagent (catalog number MIR 50115) from Mirus Bio, and cells were used for experiments 72–96 h after transfection.

Immunoprecipitation—Isolated neonatal mouse ventricular cardiomyocytes from four 100-mm diameter dishes or adult mouse myocytes (~2 mg of protein) were rinsed with ice-cold TBS (pH 7.4) and lysed in ice-cold solubilization buffer containing 25 mM Tris-HCl (pH 7.4), 150 mM NaCl, 60 mM *n*-octyl D-glucoside, 1% Triton X-100, 2 mM phenylmethylsulfonyl fluoride, 5 μg/ml of aprotinin, 5 μg/ml of benzamidin, 5 μg/ml of leupeptin, and 5 μM pepstatin A. The lysate was centrifuged at 10,000 $\times$ *g* for 10 min to remove insoluble debris, and the soluble supernatant was pre-cleared using protein G-Dynabeads (Invitrogen), followed by incubation for 4 h at 4 °C with anti-Cav-3 (5 μg) or anti-$Ca_v3.1$ or $Ca_v3.2$ (5 μg) antibodies or control IgG in a total of 450 μl. 50 μl of 1:1 slurry of protein G-Dynabeads was added to the sample and further incubated for 1 h at 4 °C. Beads were washed four times with solubilization buffer on a magnetic stand, and bound proteins were eluted with SDS-PAGE sample buffer by boiling for 5 min. Immune complexes were analyzed by SDS-PAGE (4–15% gradient gels, Bio-Rad) and Western blot by probing with antibodies to $Ca_v3.1$, $Ca_v3.2$, and Cav-3.

Cav-3 Subdomain Plasmids, GST-Cav-3 Fusion Plasmids, and Pulldown Assays—Full-length and different subdomains of Cav-3 were generated by standard polymerase chain reaction strategies utilizing the human Cav-3 as template. cDNA clones were constructed of the Cav-3 N terminus domain (amino acids 1–54, Cav-3^{1-54}), scaffolding domain (amino acids 55–74, Cav-3^{55-74}), membrane domain (amino acids 75–107, Cav-3^{75-107}), and C-terminal domain (amino acids 108–151, Cav-$3^{108-151}$). The amplified product was cloned into pcDNA3.1 with a TOPO directional cloning system reagent kit from Invitrogen according to the manufacturer's instructions and transformed into *Escherichia coli* BL21 strain. The plasmid DNA was purified using a Plasmid Maxi kit (Qiagen). DNA sequencing was used to confirm the correctness of the domains. For generations of Cav-3-GST fusion proteins the PCR products were subcloned into *Pme1* and *Sgf1* sites of pFN2A (GST) Flexi vector (Promega) by restriction digestion. The resulting wild-type and truncated Cav-3 constructs were confirmed by sequencing and transformed into *E. coli* BL21(DE3) strain. The GST fusion protein was purified from *E. coli* following induction by 0.1 mM isopropyl 1-thio-β-D-galactopyranoside and linked to glutathione-agarose beads as described earlier (31, 32). For pulldown assays, $Ca_v3.2$ channel protein was expressed in HEK293 cells, 48 h after transfection the cells were lysed and solubilized on ice using ice-cold solubilization buffer (10 mM Tris, 150 mM NaCl, 5 mM EDTA, 1% Nonidet P40, 1% Triton X-100, 60 mM *N*-octylglucoside, 2 μM phenylmethylsulfonyl fluoride, 1 μg/ml of aprotinin, 2 μg/ml of benzamidin, 1 μg/ml of leupeptin, and 1 μg/ml of pepstatin A), the lysate was then centrifuged at 10,000 $\times$ *g* for 10 min. The soluble supernatant was collected and then allowed (2 mg of protein) to bind to the MagneGST-agarose beads (Promega) linked with different Cav-3 GST fusion protein constructs. After a 4-h incubation at 4 °C, the sample was washed in 20 mM Tris, 150 mM NaCl, 5 mM EDTA, 0.1% Triton X-100, 0.5% sodium deoxycholate. The eluted sample was then separated and analyzed by SDS-PAGE and Western blot, respectively, by probing with anti-$Ca_v3.2$ (1:100, rabbit polyclonal, Alomone Labs) and anti-GST antibody (1:500, mouse monoclonal; BD Biosciences).

SDS-PAGE and Western Blot Analysis—Myocyte lysates, or the immune complexes were separated by SDS-PAGE (4–15% gradient acrylamide gel) and transferred to polyvinylidene difluoride membranes. Nonspecific binding sites were blocked by 5% (w/v) dried skim milk in TBS detergent (0.1% Tween 20). Membranes were then probed with specific primary antibodies ($Ca_v3.1$ or $Ca_v3.2$, 1:100; Cav-3, 1:1000) followed by a washing step (four times for 10 min each) with TBS detergent. The membranes were then incubated with either goat anti-mouse Ig conjugated to horseradish peroxidase (1:10,000) or goat anti-rabbit IgG to horseradish peroxidase (1:10,000; Bio-Rad) for 1 h and washed (six times for 10 min) with TBS detergent. Immunoreactivity was visualized using peroxidase-based chemiluminescent detection by ECL (Amersham Biosciences).

Biotinylation of Cell Surface Protein and Immunoblotting—Surface biotinylation studies were performed as described earlier (33) in HEK293 cells stably expressing $Ca_v3.2$ channel protein. Briefly, HEK293 cells stably expressing $Ca_v3.2$ channels were grown in 100-mm culture dishes and transfected with Cav-3 or GFP. After 48 h, cells were washed three times with PBS and incubated with sulfo-NHS-(LC)-biotin (0.5 mg/ml; Pierce) in PBS at 4 °C for 1 h. Cells were then washed five times with ice-cold PBS to remove residual biotin reagent and solubilized in lysis buffer with protease inhibitors. Lysate pro-

teins were quantified with a bicinchoninic acid assay (Pierce). Proteins (0.5 mg/reaction) were mixed with anti-Cav3.2 antibody (5 μg) immunoprecipitated using the protein G-Dynabeads as described above. The immunoprecipitated sample was analyzed by Western blotting by probing with anti-biotin antibody (mouse monoclonal, 1:5,000, BD Biosciences). Immunoblot membrane was then stripped and re-probed with anti-$Ca_v3.2$ antibody (1:100) to detect the $Ca_v3.2$ channel protein signal.

Adenoviral Infection of $Ca_v3.2$ Channel—Adenoviruses expressing either $Ca_v3.2$ channel protein (AdCav3.2) or green fluorescent protein (AdGFP) were amplified as described by Brueggemann *et al.* (34). Isolated neonatal mouse ventricular myocytes were plated on laminin-coated coverslips in a 35-mm Petri dish at 1×10^5 cells and infected with Ad$Ca_v3.2$ or AdGFP at a multiplicity of infection of 5–10. More than 90% cells infected with Ad-GFP expressed GFP 48 h after infection. Negligible cell death was observed in cultures infected with adenovirus. Experiments were performed 72–96 h after adenoviral infection.

siRNA-mediated Cav-3 Knockdown—siRNA-mediated knockdown of Cav-3 in isolated neonatal mouse cardiomyocytes was archived by transfecting three pairs of pre-validated Cav-3 specific siRNAs as described earlier (24). Cav-3 sequences targeting different regions for mouse Cav-3 (GenBank™ accession number NM_007617; sense, GCUUCGACGGUGUAUGGAAtt, and antisense, UUCCAUACACCGUCGAAGCtg; sense, GGUUCCUCUCAAUUCCACCtt, and antisense GGUGGAAUUGAGAGGAACCtc; sense, CGUUCACCGUCUCCAAGUtt, and antisense, UACUUGGAGACGGUGAACGtg) were used for Cav-3 knockdown. Nonspecific siRNA oligos to mouse GAPDH (Applied Biosciences) was used as controls. Briefly, freshly isolated neonatal mouse myocytes were transfected by the electroporation method with the desired oligos (10 nM) and 0.5 μg of cDNA for GFP as previously described (24). Forty-eight to 72 h after transfection myocytes was evaluated for GFP expression and immunostained for Cav-3 (rabbit polyclonal antibody; Santa Cruz Biotechnology 1:500 dilution) and cardiac-specific actin (mouse monoclonal antibody; BD Biosciences; 1:1000 dilution) expression to determine Cav-3 knockdown in the myocytes. The number of GFP-expressing cells divided by the total number of cells in the field of view determined transfection efficiency (data not shown) and was estimated to be between 50 and 60%. Neonatal myocytes expressing GFP fluorescence were used for patch clamp experiments.

Transthoracic Aortic Constriction (TAC)-induced Pressure Overload and Echocardiography Analysis—TAC was performed on 8–12-week-old C57BL/6 male mice as described previously (35). Sham-operated mice were subjected to identical interventions except for the constriction of the aorta. Noninvasive transthoracic echocardiography (35) was performed before and after 4 weeks of TAC surgery in mice, and LV wall thickness, chamber dimension, and contractility were evaluated. The pressure gradients across the aortic constriction were measured to ensure similar pressure overload in the TAC mice.

Immunogold Labeling and Electron Microscopy—Double immunogold labeling co-localization studies and electron microscopy (EM) was performed on isolated and cultured neonatal myocytes as described by Balijepalli *et al.* (24) using anti-$Ca_v3.2$ (rabbit polyclonal) and anti-Cav-3 (mouse monoclonal) antibodies and a double silver enhancement technique.

Electrophysiology—Electrophysiological recordings were made from HEK293 cells transiently expressing human cardiac T-type calcium channels ($I_{Cav3.1}$ and $I_{Cav3.2}$) and Cav-3 as described previously (28). T- and L-type calcium currents were recorded from cultured mouse neonatal cardiomyocytes (3–5 days *in vitro*). Calcium currents were measured from isolated cells with bright GFP fluorescence with either ruptured or perforated patch configuration. The patch pipettes were pulled from thin walled borosilicate glass capillaries (World Precision Instruments, Inc., Sarasota FL) and filled with an intracellular solution containing the following (in mM) for both HEK293 cells and neonatal cardiomyocytes: 114 CsCl, 10 EGTA, 10 HEPES, 5 MgATP (pH 7.2) adjusted with CsOH. Extracellular buffer for HEK293 cells contained the following (in mM): 128 CsCl, 2 $CaCl_2$, 1.5 $MgCl_2$, 10 HEPES, 25 D-glucose (pH 7.4), adjusted with CsOH. For neonatal cardiomyocytes (in mM): 145 tetramethylammonium chloride, 5 $CaCl_2$, 1 $MgCl_2$, 5 CsCl, 1,4-aminopyridine, 0.01 tetrodotoxin, 10 HEPES, 5 D-glucose (pH 7.4), adjusted with tetramethylammonium OH. The current-voltage relationship was evoked by step depolarization from −90 to +60 mV with 10-mV step voltage for 200 ms. For perforated patch clamp measurements the pipette solution contained (in mM): 140 Cs-glutamate, 10 HEPES, 0.5 $CaCl_2$, and 400 μg/ml of amphotericin B (pH 7.2). The external buffer consists of (in mM): 145 tetramethylammonium chloride, 5 $CaCl_2$, 1 $MgCl_2$, 10 HEPES, and 5 D-glucose, 5 CsCl, 1 aminopyridine, and tetrodotoxin (1 μM) bath applied. The peak $I_{Ca,T}$ were measured at a holding potential at −90 mV, a test pulse of −30 mV for 200 ms was applied at 15-s time intervals. After the initial basal $I_{Ca,T}$ measurement, 3–5-min myocytes were perfused with 100 μM 8-Br-cAMP (in the bath solution) to activate the protein kinase A (PKA)-dependent stimulation of the $I_{Ca,T}$. Following stimulation with 8-Br-cAMP, 10 μM nitrendipine and 0.5 mM NiCl were included in the bath solution to block $I_{Ca,L}$ and $I_{Ca,T}$, respectively. In some experiments neonatal myocytes were pretreated with 10 μM myristoylated PKA inhibitor peptide (overnight incubation) to inhibit the PKA activity. The data were collected from a minimum of three different transfections. All experiments were carried out at room temperature with pipette resistance of 1.5–2.5 MΩ. The data were acquired using Axopatch 200B amplifier (Axon Instruments, Foster City, CA) with pCLAMP 10.2. The data were filtered at 5 kHz and digitized at 50 kHz. The current traces were corrected for linear capacitance and leak using -P/4 subtraction protocol.

Data Analysis—Data were analyzed using the Clampfit and Origin 7.5 software programs. The curves for steady state activation and inactivation were fitted using Boltzmann equation. The current-voltage curves were fitted using the Boltzmann function: $I = I_{max}/(1 + \exp[-(V - V_{1/2})/k])$. All the

results are presented as the mean ± S.E. and the significance of the observed difference was evaluated by unpaired Student's *t* test. *p* value of <0.05 was considered statistically significant.

RESULTS

T-type Ca^{2+} Channel Isoforms Associate with Cav-3 in Ventricular Myocytes and HEK293 Cells—T-type Ca^{2+} channel isoforms $Ca_v3.1$ and $Ca_v3.2$ as well as Cav-3 are known to be expressed in neonatal cardiomyocytes. To determine whether Cav-3, $Ca_v3.1$, and $Ca_v3.2$ channels are associated in ventricular myocytes, we performed co-immunoprecipitation experiments. Lysates from isolated neonatal mouse ventricular myocytes were solubilized in Triton X-100 and *N*-octyl D-glucoside-containing buffer and subjected to immunoprecipitation with anti-Cav-3 or control mouse IgG. Western blot analysis shows that $Ca_v3.1$ and $Ca_v3.2$ protein bands were detected from the mouse neonatal myocytes lysate (Fig. 1, *A* and *B*). Both TTCC isoforms co-immunoprecipitated with Cav-3 from neonatal mouse ventricular myocytes lysates. In a converse experiment we used either anti-$Ca_v3.1$ or $Ca_v3.2$ or a control rabbit IgG antibody for immunoprecipitation from neonatal ventricular myocyte lysates and found that Cav-3 co-immunoprecipitated with either of the TTCC isoform antibodies but not with control IgG. These results suggested that the $Ca_v3.1$ and $Ca_v3.2$ channels associate with Cav-3 in ventricular myocytes. To further confirm these results in a heterologous expression system we transiently expressed Cav-3 and $Ca_v3.1$ or $Ca_v3.2$ channel proteins in HEK293 cells that do not express either of these proteins endogenously. 48 h post-transfection cell lysates were subjected to immunoprecipitation with anti-Cav-3, or control mouse IgG. As demonstrated in Fig. 1*C*, the T-type Ca^{2+} channel isoform $Ca_v3.1$ and $Ca_v3.2$ proteins co-immunoprecipitated with anti-Cav-3 antibody. These results confirmed that the T-type Ca^{2+} channels associate with Cav-3. Non-transfected HEK293 cells did not show protein bands for T-type Ca^{2+} channel isoforms or Cav-3.

$Ca_v3.2$ Channel Protein Co-localized with Cav-3 Relative to Caveolae in Ventricular Myocytes—To determine the precise localization of $Ca_v3.2$ channels we used the immunogold labeling technique combined with electron microscopy. To determine localization of the $Ca_v3.2$ channels, we initially used isolated mouse neonatal ventricular myocytes that were fixed and immunogold co-labeled with anti-Cav-3 and anti-$Ca_v3.2$ antibody. Transmission electron micrographs revealed two distinct populations of different sized gold particles (Fig. 2) present on surface membrane invaginations typical of caveolae. The small gold particles identify anti-Cav-3 labeling (*arrows*) and large gold particles (as a result of double silver enhancement, *arrowhead*) identify anti-$Ca_v3.2$ channel protein labeling suggesting the co-localization of the $Ca_v3.2$ with Cav-3 relative to caveolae (Fig. 2, *a* and *c*). Immunogold labeling showed labeling for Cav-3 but did not show $Ca_v3.2$ channel staining in the ventricular myocytes of normal mouse adult heart tissue as, cardiac T-type Ca^{2+} channel isoforms are normally expressed during development but not expressed in the adult hearts (Fig. 2, *e* and *g*). However, these

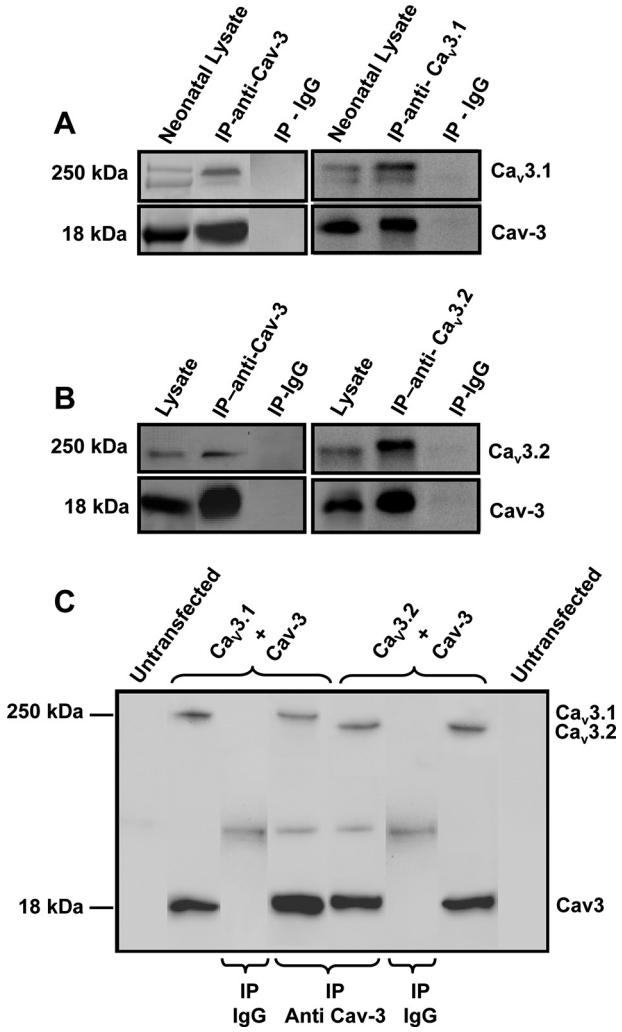

FIGURE 1. **T-type calcium channel isoforms $Ca_v3.1$ and $Ca_v3.2$ associate with Cav-3.** Neonatal mouse myocyte homogenates were subjected to immunoprecipitation with either anti-$Ca_v3.1$ or $Ca_v3.2$ or Cav-3 antibodies, and the immunoprecipitates were analyzed by immunoblotting. *A*, representative immunoblot showing $Ca_v3.1$ and Cav-3 detected in the immunoprecipitates with either of the two antibodies, whereas control IgG does not immunoprecipitate the proteins. *B*, representative immunoblot showing $Ca_v3.2$ and Cav-3 detected in the immunoprecipitates with either of the two antibodies, whereas control IgG does not immunoprecipitate the proteins. *C*, representative immunoblot showing co-immunoprecipitation of $Ca_v3.1$ and $Ca_v3.2$ proteins from transiently expressed HEK293 cell lysates using anti-Cav-3 antibody. Both $Ca_v3.1$ and $Ca_v3.2$ channel proteins co-immunoprecipitate with anti Cav-3 antibody, whereas control IgG does not immunoprecipitate either protein. Signal for $Ca_v3.1$ and $Ca_v3.2$ channel proteins was not detected in the untransfected HEK293 cell lysates. Results are representative of 4 different experiments.

channels are known to re-express during pressure overload-induced cardiac hypertrophy and heart failure (11–15). Adult mice were subjected to the TAC procedure to generate pressure overload-induced cardiac hypertrophy. Echocardiography analysis (supplemental Table S1) confirmed induction of cardiac hypertrophy. Adult hearts were fixed by perfusion fixation and co-immunogold labeling was performed. As shown in the transmission electron micrograph (Fig. 2, *b* and *d*), $Ca_v3.2$ channel protein (large gold particle) and Cav-3 (small gold particle) were co-localized relative to caveolae. Also, the gold particle distribution was restricted to sarcolemma regions in the ventricular myocytes suggesting specific

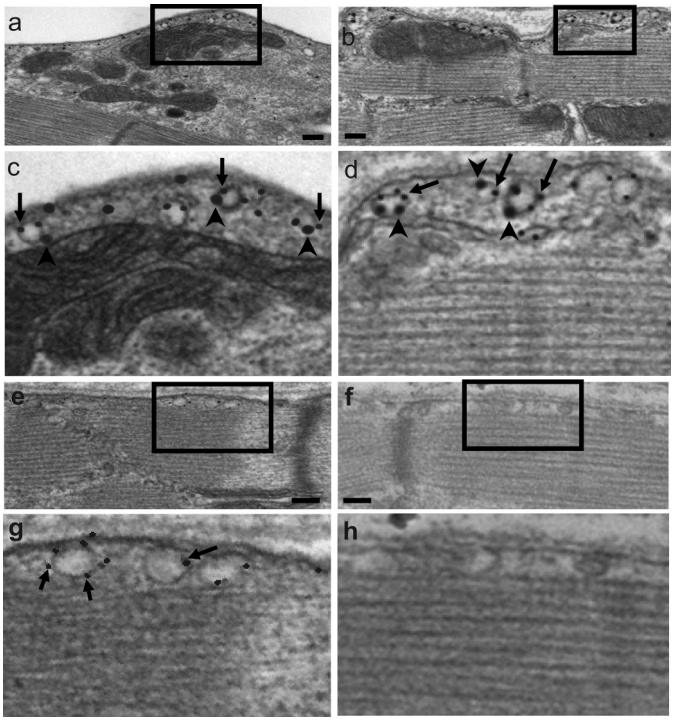

FIGURE 2. **$Ca_v3.2$ and Cav-3 are colocalized relative to caveolae in mouse ventricular myocyte.** Representative transmission electron micrographs show immunogold labeling for $Ca_v3.2$ (large particle, *arrowhead*) and Cav-3 (small particle, *arrow*) in neonatal cardiomyocyte (*a* and *c* are enlarged) and hypertrophic adult ventricular myocytes (*b* and *d* are enlarged). Normal adult ventricular myocytes show staining for Cav-3 but not for $Ca_v3.2$ (*e* and *g* are enlarged). Control image in *f* (portion enlarged in *h*) shows no primary antibody from hypertrophic adult ventricular myocyte. *Scale bars*, 100 nm.

caveolar localization of the protein. In control samples (hypertrophic adult mouse heart) from which the primary antibodies had been omitted, did not show gold particle staining.

Co-expression of Cav-3 Inhibits $I_{Cav3.2}$ but Not $I_{Cav3.1}$ in HEK293 Cells—To determine the functional impact of Cav-3 association on T-type Ca^{2+} channel currents we used a heterologous system of HEK293 cells, which provides a convenient expression system to study specific transfected T-type Ca^{2+} channels and Cav-3, given the lack of endogenous expression of these proteins. HEK293 cells have been used by us and others to study the heterologous expression of T-type Ca^{2+} channels and a wide array of other ion channels (28, 29, 36–39). Human TTCC isoforms $Ca_v3.1$ and $Ca_v3.2$ were separately co-expressed with Cav-3 in HEK293 cells and the respective currents were measured using the whole cell patch clamp technique. Currents were measured from a holding potential of −90 mV and stepped to 60 mV in 10-mV increments for 200 ms (as shown in the Fig. 3, *B* and *inset D*). Fig. 3, *B* and *D,* shows the current-voltage relationship of $I_{Cav3.1}$ and $I_{Cav3.2}$, respectively, with and without co-expression of Cav-3. Co-expression of Cav-3 did not effect the $I_{Cav3.1}$ (-32.8 ± 5 pA/pF, $n = 11$) compared with expression of $Ca_v3.1$ with GFP (−33.48 ± 4 pA/pF, $n = 11$). On the other hand co-expression of Cav-3 with $Ca_v3.2$ significantly reduced $I_{Cav3.2}$ (−11.48 ± 3 pA/pF, $n = 11$) compared with $Ca_v3.2$ + GFP (−31 ± 4 pA/pF, $n = 11$). We also investigated the effect of co-expression of Cav-3 on the biophysical properties of the $I_{Cav3.2}$ in HEK293 cells. Co-expression of Cav-3 did not affect $Ca_v3.2$ channel activation and inactivation properties. These data are presented in supplemental Fig. S1.

Effect of Co-expression of Cav-3 on Plasma Membrane Expression of $Ca_v3.2$ Channel Protein—To understand the mechanism of Cav-3 inhibition of the $I_{Cav3.2}$ we investigated if Cav-3 co-expression alters trafficking and reduces the surface expression of the $Ca_v3.2$ channels. One way to determine the number of channels expressed on the plasma membrane is to measure the gating currents, however, given the small $I_{Cav3.2}$ amplitudes (300–500 pA) we could not measure the gating currents to estimate the number of plasma membrane-expressed $Ca_v3.2$ channels with Cav-3 co-expression. We used an alternative approach of cell surface biotinylation of the $Ca_v3.2$ channels. HEK293 cells were transfected with cDNAs of $Ca_v3.2$ + GFP or $Ca_v3.2$ + Cav-3, or GFP alone. Cell lysates were precipitated with neutravidin beads and samples were analyzed by Western blots by probing with anti-$Ca_v3.2$ or anti-β-actin antibody. As shown in a representative Western blot (Fig. 3*E*), no difference was noticed in the biotinylated $Ca_v3.2$ protein signal intensity when $Ca_v3.2$ was expressed alone ($Ca_v3.2$ + GFP) or co-expressed with Cav-3 ($Ca_v3.2$ + Cav-3) suggesting that co-expression of Cav-3 did not affect the surface membrane expression of $Ca_v3.2$ channel. These experiments were repeated three times and the signal for the biotinylated $Ca_v3.2$ band was semi-quantitatively estimated by densitometry. We found that the mean signal density for the biotinylated $Ca_v3.2$ band was not different between groups (data not shown). The $Ca_v3.2$ protein signal was absent in the sample that was transfected with GFP alone. We did not detect a signal for β-actin, demonstrating the biotinylation of only surface membrane proteins. The signal for Cav-3 as also absent in the neutravidin pulldown as Cav-3 is localized to the inner leaflet of the plasma membrane bilayer and not biotinylated. A portion of the lysate sample from 3 groups was also analyzed by probing with anti-$Ca_v3.2$ and anti-β-actin (Fig. 3, *panel F*) for loading control. Again similar signal intensity for the $Ca_v3.2$ channel protein was detected with either $Ca_v3.2$ alone or with co-expression of Cav-3 and a similar β-actin signal was detected between the three groups of cells demonstrating identical sample loading.

$Ca_v3.2$ Interaction Site on Cav-3—We next examined the site of interaction for Cav-3 with the $Ca_v3.2$ channel protein. We created five different GST fusion constructs of Cav-3 based on known domains (illustrated in Fig. 4*A* and see Ref. 18): 1) full-length (Cav-3FL), 2) Cav-3Nterm (Cav-3^{1-54}), 3) Cav-3Scaf (Cav-3^{55-73}), 4) Cav-3Mem (Cav-3^{74-106}), and 5) Cav-3Cterm domain (Cav-$3^{107-151}$) using a bacterial system as described under "Experimental Procedures." $Ca_v3.2$ channel protein was expressed in HEK293 cells, and the lysates were incubated with GST alone or different GST-Cav-3 fusion proteins linked to glutathione beads. Following that procedure, a pulldown assay was performed and samples were analyzed by Western blotting. As demonstrated in Fig. 4*B*, the $Ca_v3.2$ channel was found to interact and associate with the full-length GST fusion protein of Cav-3 (GSTCav-3FL) and N terminus GST fusion protein of Cav-3 (GST-Cav3NT; amino acids 1–54) but not associate with GST-Cav-3Scaf

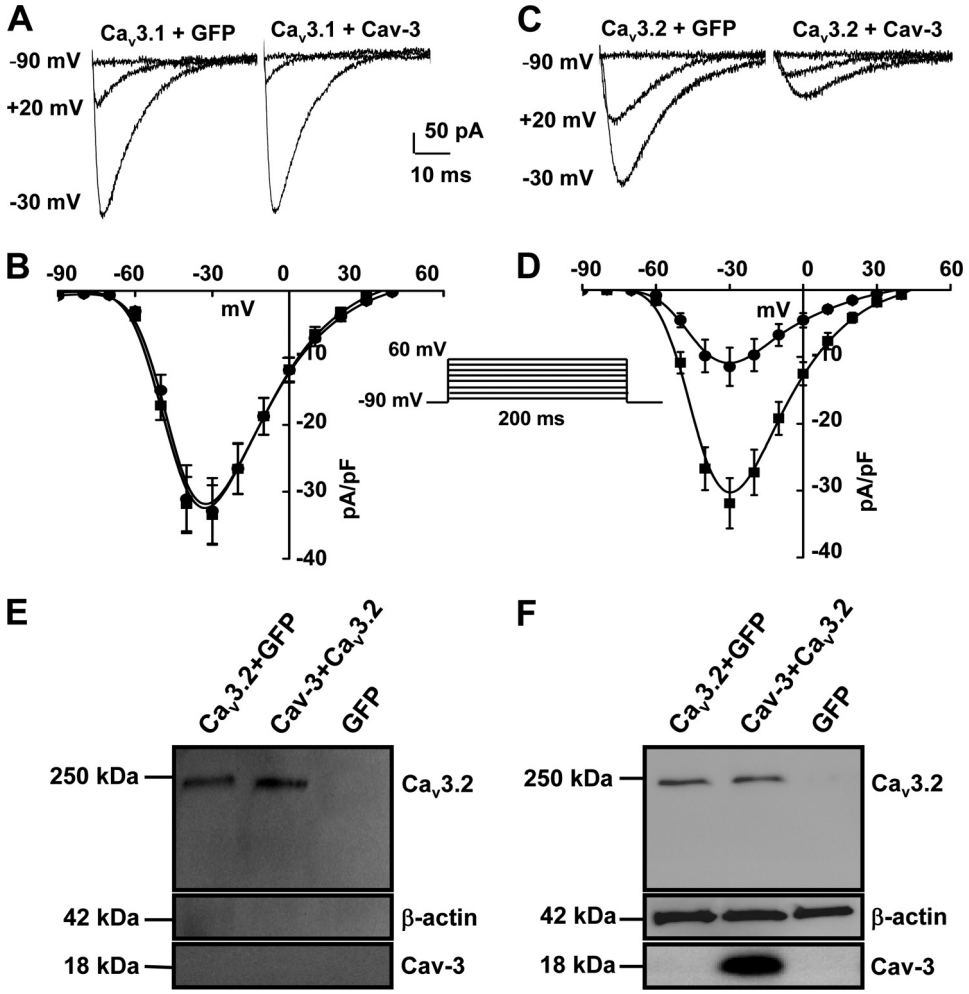

FIGURE 3. **Co-expression of Cav-3 inhibits $I_{Cav3.2}$ but not $I_{Cav3.1}$ in HEK293 cells.** Whole cell voltage clamp recordings of T-type Ca^{2+} were performed in HEK293 cells expressing either $Ca_v3.1$ or $Ca_v3.2$ alone or co-expressing with Cav-3, by using a holding potential of −90 mV and step pulsed to 60 at 10 mV as shown in the *inset*. *A*, representative whole cell Ca^{2+} current traces at −90, −30, and +20 mV from transiently transfected HEK293 cells with $Ca_v3.1$ alone and $Ca_v3.1$ with Cav-3. *B*, average current density plotted against the change in test potential for $Ca_v3.1$ (■) alone and with $Ca_v3.1$ + Cav3 (●). *C*, representative whole cell Ca^{2+} current traces at −90, −30, and +20 mV from transiently transfected HEK293 cells with $Ca_v3.2$ alone and $Ca_v3.2$ with Cav-3. *D*, average current density plotted against the change in test potential for $Ca_v3.2$ (■) alone and with $Ca_v3.2$ + Cav-3 (●). Data represents mean ± S.E. (n = 11 from 4 different transfections). Co-expression of Cav-3 does not alter plasma membrane expression of $Ca_v3.2$ channel protein. HEK293 cells were transfected with cDNAs of $Ca_v3.2$ + GFP or $Ca_v3.2$ + Cav-3 or GFP alone. *E*, cell lysates were precipitated with neutravidin beads and the sample was analyzed by Western blots by probing with anti-$Ca_v3.2$ or anti-β-actin antibodies as indicated in the representative immunoblot. Similar signal intensity for the biotinylated $Ca_v3.2$ protein was detected with $Ca_v3.2$ + GFP or $Ca_v3.2$ + Cav-3. *F*, a portion of the total lysate (50 μl) sample as input from 3 groups was also analyzed by probing with anti-$Ca_v3.2$ and anti-β-actin for loading control. Similar signal intensity for the $Ca_v3.2$ channel protein was detected with either $Ca_v3.2$ alone or with co-expression of Cav-3 and similar β-actin signal was detected between the three groups of cells demonstrating identical sample loading. Data are representative of three different experiments.

(Cav-3^{55-73}), GST-Cav-3Mem (Cav-3^{74-106}), and the GST-Cav-3C-terminus domain (Cav-$3^{107-151}$). This suggested that the $Ca_v3.2$ subunit interacts with Cav-3 and specifically interacts with the N-terminal region of the Cav-3.

Co-expression of Cav-3 N Terminus Domain Inhibits $I_{Cav3.2}$ in HEK293 Cells—Our GST pulldown assay demonstrates that the N terminus of Cav-3 interacts with the $Ca_v3.2$ channel. To determine the functional impact of this interaction on $Ca_v3.2$ channels, we generated cDNA constructs of the N terminus region (Cav-3^{1-54}) and other regions of Cav-3 as described under "Experimental Procedures." These cDNAs along with the $Ca_v3.2$ cDNA were then transiently transfected into HEK293 cells. $I_{Cav3.2}$ was then measured by whole cell patch clamp analysis. As demonstrated in Fig. 4*B*, co-expression of Cav-3Nterm significantly reduced the $I_{Cav3.2}$ (11.7 ± 1 pA/pF, n = 7) compared with $Ca_v3.2$ alone (24.1 ± 2 pA/pF, n = 7). On the other hand co-expression of Cav-3Cterm, Cav-3Scaf, or Cav-3Memb with $Ca_v3.2$ channels did not alter the $I_{Cav3.2}$. These data further demonstrate that interaction of the N terminus region of Cav-3 with the $Ca_v3.2$ channel protein modulates the channel function.

Overexpression of Cav-3 Inhibits $I_{Ca,T}$ in Mouse Neonatal Ventricular Myocyte—Our data from the heterologous expression system of HEK293 cells demonstrated that co-expression of Cav-3 specifically inhibited the $I_{Cav3.2}$. Next we investigated if Cav-3 will have a similar effect on the native T-type Ca^{2+} current ($I_{Ca,T}$) using isolated neonatal cardiomyocytes where Cav-3 and the $Ca_v3.2$ channel isoform are endogenously expressed. Neonatal ventricular myocytes express both isoforms of TTCC as well as $Ca_v1.2$, L-type Ca^{2+} chan-

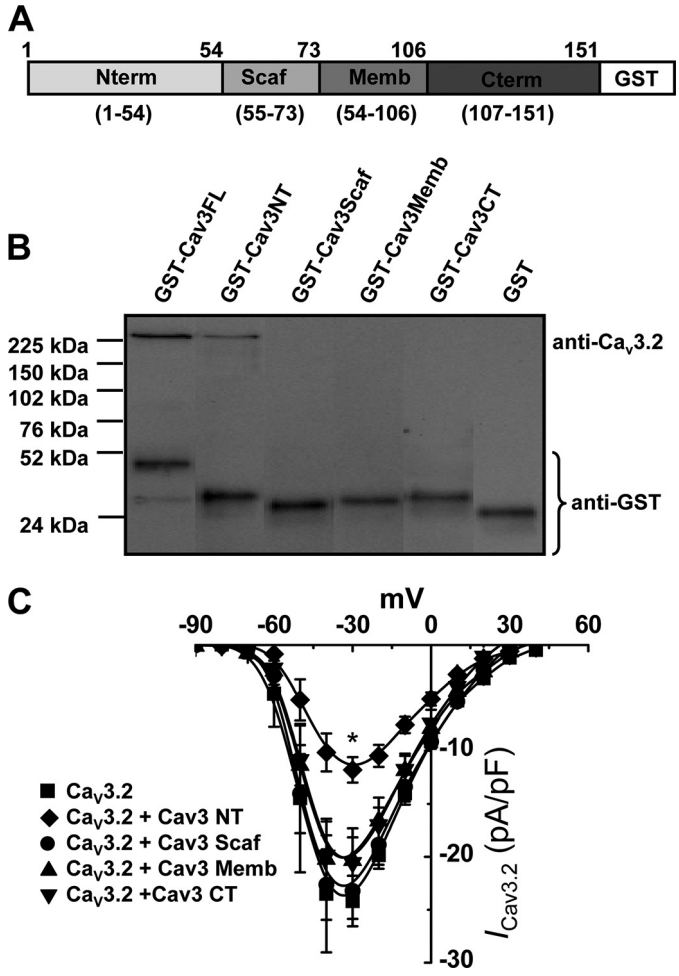

FIGURE 4. **N terminus region of Cav-3 interacts with $Ca_v3.2$ channel protein and inhibits $I_{Cav3.2}$.** *A*, diagram of the domain structure of Cav-3. GST was fused with full-length Cav-3 and the different Cav-3 domains and tested for an ability to interact with the $Ca_v3.2$ channel. *B*, representative Western blot analyses of the GST pulldown assay. $Ca_v3.2$ channels were expressed in HEK293 cells, and lysates were incubated with different GST-Cav-3 fusion proteins as described under "Experimental Procedures": full-length (*GST-Cav-3FL*), Cav-3 N terminus (*GST-Cav-3NT*), Cav-3 scaffolding domain (*GST-Cav-3Scaf*), Cav-3 membrane domain (*GST-Cav-3Memb*), Cav-3 C terminus domain (*GST-Cav-3CT*), or GST alone. The pulldown samples were analyzed by probing with anti-GST and anti-$Ca_v3.2$ antibodies. *C*, HEK cells were transiently expressed with $Ca_v3.2$ alone or $Ca_v3.2$ with different Cav-3 domains (*Cav-3NT*, *Cav-3Scaf*, *Cav-3CT*, and *Cav-3Memb*). $I_{Cav3.2}$ density was measured by the whole cell patch clamp technique and plotted against a change in test potentials. Data represent mean ± S.E. ($n = 7$ each, *, $p > 0.005$ with respect to control) from three different transfections.

nels. T-type Ca^{2+} channels can be distinguished from L-type Ca^{2+} channels on the basis of their conductance and gating properties (40). The TTCCs are known to activate at significantly more negative membrane voltage potentials with a threshold for activation of I_{CaT} about −60 mV and peak I_{CaT} between −30 mV at physiological Ca^{2+} concentrations (1, 9, 16), whereas the $Ca_v1.2$ channels begin to activate at about −30 mV and the peak $I_{Ca,L}$ is elicited at more positive potentials (10 mV) (24). To isolate the pure $I_{Ca,T}$ from high voltage-activated L-type currents we used a dual pulse protocol as described earlier (16). Using a whole cell patch clamp technique (Fig. 5) the total I_{Ca} ($I_{Ca,Tot}$) was recorded from myocytes using a holding potential of −90 mV and pulsed to 60 mV in 10-mV steps for 200 ms, followed by a brief holding potential of −50 mV and further pulsed to 70 mV in a 10-mV steps for 200 ms to record the $I_{Ca,L}$. To obtain the $I_{Ca,T}$, traces of $I_{Ca,L}$ (holding potential −50 mV; Fig. 5, *B* and *C*) were subtracted from the corresponding trace of $I_{Ca,Tot}$ with a holding potential of −90 mV. Thus we found that peak $I_{Ca,T}$ was at −30 mV in these cells. Cav-3 or GFP alone were overexpressed in the isolated mouse neonatal ventricular myocytes by electroporation as described earlier (24). Using the same dual pulse protocol we measured the $I_{Ca,Tot}$, $I_{Ca,L}$, and then obtained $I_{Ca,T}$ by subtraction as demonstrated in Fig. 5, and found that the average peak $I_{Ca,T}$ density for nontransfected cells (−5 ± 0.7 pA/pF, $n = 11$) or GFP-transfected cells (−4.7 ± 1 pA/pF, $n = 11$) was similar (Fig. 5*E*). On the other hand overexpression of Cav-3 significantly reduced the $I_{Ca,T}$ 42% (−2.1 ± 1 pA/pF, $n = 8$) compared with GFP-transfected control cells (Fig. 5, *D* and *E*). Overexpression of Cav-3 had no impact on the average peak $I_{Ca,L}$ density (Fig. 5*F*).

Neonatal ventricular myocytes express $Ca_v3.1$ and $Ca_v3.2$ and kinetic properties of $I_{Cav3.1}$ and $I_{Cav3.2}$ closely resemble native I_{CaT}. Thus it is difficult to differentiate between the two different current components in a native cardiomyocyte system based on their biophysical properties. Studies have shown that $I_{Cav3.1}$ and $I_{Cav3.2}$ can be differentiated by their sensitivity to block by Ni^{2+}. Recombinant $Ca_v3.2$ channel is shown to be blocked by low concentrations of Ni^{2+} ($IC_{50} = 12\ \mu M$), whereas the $Ca_v3.1$ channel is blocked by higher concentrations of Ni^{2+} ($IC_{50} = 250\ \mu M$) (41). However, in our conditions we did not find it practical to use Ni^{2+} to differentiate between the components of TTCCs because a higher concentration of Ni^{2+} is needed to block $I_{Cav3.1}$. So we used an adenoviral overexpression model of $I_{Cav3.2}$ and studied the effect of Cav-3 on the $I_{Ca,T}$. Isolated neonatal myocytes were transfected with either Cav-3 or GFP alone as above and then infected with $AdCa_v3.2$ or AdGFP. Overexpression of $Ca_v3.2$ proteins was confirmed by Western blot analysis (data not shown) and by measuring $I_{Cav3.2}$. $AdCa_v3.2$-treated cells showed significantly increased $I_{Cav3.2}$ (-32.4 ± 7 pA/pF) compared with AdGFP-treated control cells (−4.9 ± 1 pA/pF) or non-treated control cells (Fig. 6*A*). Co-expression of Cav-3 significantly reduced (89%) the $AdCa_v3.2$-induced $I_{Cav3.2}$ (−4.37 ± 1pA/pF), suggesting that Cav-3 inhibits and regulates that $I_{Cav3.2}$ in neonatal cardiomyocytes. $AdCa_v3.2$ or AdGFP treatment did not alter the average $I_{Ca,L}$ density in the neonatal ventricular myocytes (Fig. 6*B*).

To determine the involvement of Cav-3 on the modulation of $Ca_v3.2$ channels in neonatal cardiomyocytes, we investigated the impact of the specific inhibition of Cav-3 expression using siRNA-mediated gene silencing as described earlier (24). Three different siRNA oligos specific to mouse Cav-3 or control siRNA to GAPDH were co-transfected with GFP into isolated mouse neonatal cardiomyocytes. 72 h after transfection knockdown of Cav-3 was established by Western blot analysis and immunofluorescence imaging for Cav-3, which confirmed that Cav-3 siRNA-transfected cells (GFP-expressing) exhibited near complete knockdown of Cav-3 (see supplemental Fig. S2). Whole cell electrophysiology was performed on GFP expressing cells (green fluorescence) to measure $I_{Ca,T}$. siRNA-mediated knockdown of Cav-3 did not

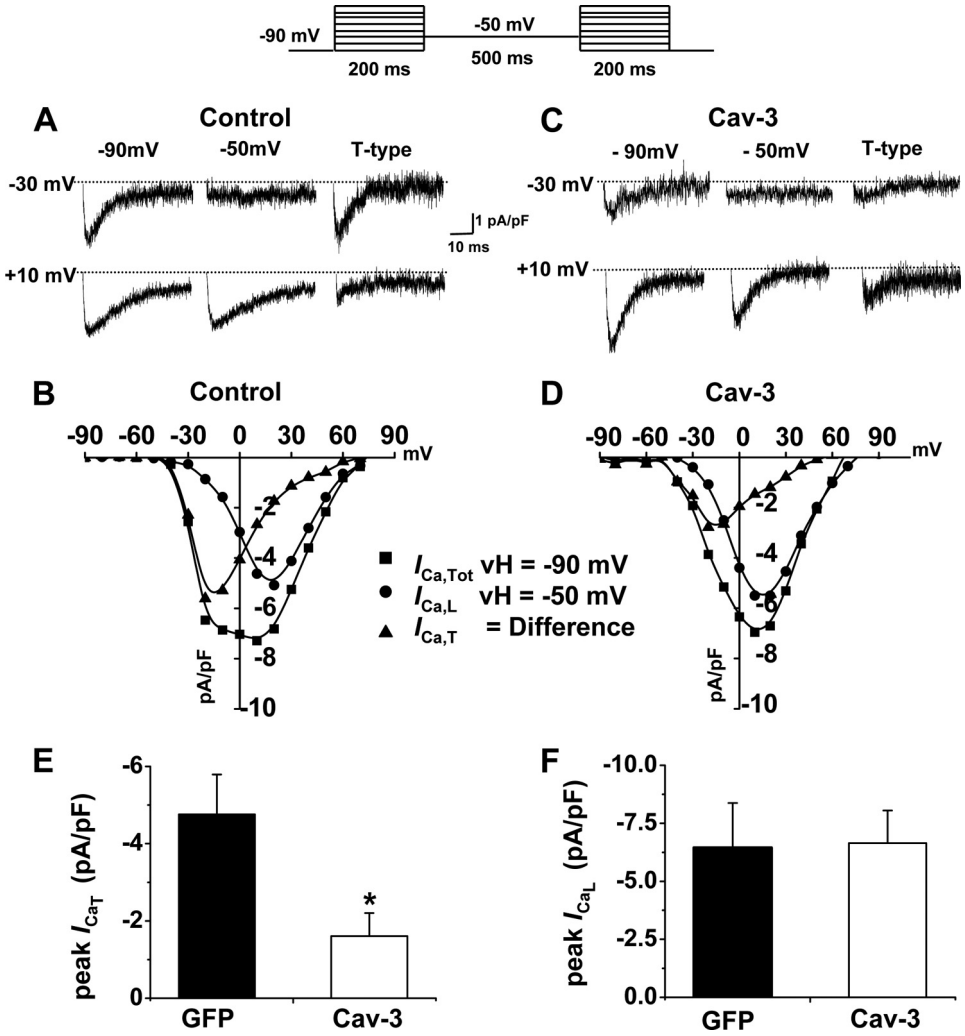

FIGURE 5. **Overexpression of Cav-3 inhibits $I_{Ca,T}$ in isolated mouse neonatal ventricular myocytes.** Whole cell patch clamp analysis was performed in neonatal myocytes transfected with Cav-3 or GFP (control) using a protocol as described under "Results" and shown in the *inset* on top. *A* and *C* show representative current traces of GFP and Cav-3-transfected cells, respectively, using a holding potential of −90 mV (*left*) and −50 mV (*middle*) to a step depolarization to the respective indicated command potential. The traces on the *right* are obtained by subtracting the middle trace from the left current trace and represent the T-type Ca^{2+} current. *Panels C* and *D*, representative current density plot generated by a series of step depolarization potentials of 10 mV at different holding potentials, *i.e.* −90 mV ($I_{Ca,Total}$, ■) and −50 mV ($I_{Ca,L}$, ●) the difference is the T-type current ($I_{Ca,T}$, ▲) in control (GFP) and Cav-3 overexpression cells, respectively. *E*, peak current density of $I_{Ca,T}$ with or without overexpression of Cav-3. *F*, peak $I_{Ca,L}$ densities with and without overexpression of Cav-3. The data represent mean ± S.E. ($n = 8–11$ cells, *, $p > 0.05$) from 3 different transfections.

alter the $I_{Ca,T}$ densities (−4.5 ± 0.8 pA/pF $n = 22$), and was similar to control (GAPDH) siRNA-transfected myocytes (−5.4 ± 1 pA/pF, $n = 21$) or nontransfected neonatal cardiomyocytes (5 ± 0.7 pA/pF, $n = 9$) (Fig. 6*C*). siRNA-mediated knockdown of Cav-3 also had no effect on the average $I_{Ca,L}$ density as shown in Fig. 6*D*. A similar effect of siRNA-mediated knockdown on the $I_{Ca,L}$ was observed in an earlier study from our group when siRNA-mediated knockdown of Cav-3 did not alter the mean $I_{Ca,L}$ current densities compared with control siRNA-treated neonatal ventricular myocytes (24).

siRNA-mediated Knockdown of Cav-3 Eliminates Protein Kinase A Regulation of the $I_{Ca,T}$ in Mouse Neonatal Myocytes—Overexpression of Cav-3 inhibited the $I_{Cav3.2}$ but the siRNA-mediated inhibition of Cav-3 expression did not affect the $I_{Ca,T}$ density in neonatal myocytes. We reasoned that Cav-3 may play an important role in regulation of $Ca_v3.2$ channels and Cav-3 knockdown may alter regulation of the $I_{Ca,T}$ in neonatal mouse cardiomyocytes. The $I_{Ca,T}$ and $I_{Cav3.2}$ are reported to be augmented by cAMP-dependent protein kinase (PKA) (42–44). We investigated the PKA regulation of the $I_{Ca,T}$ in neonatal myocytes using 8-bromo-cAMP (membrane permeable cAMP-a known activator of PKA) by perforated clamp analysis. Initially a dose-dependent stimulation of $I_{Ca,T}$ was performed with 8-Br-cAMP and we found a maximal stimulation of $I_{Ca,T}$ at 100 μM concentrations (data not shown). In the myocytes that were transfected with control siRNA, 8-Br-cAMP resulted in a PKA-mediated increased stimulation of the peak $I_{Ca,T}$ to 126 ± 6% (Fig. 7, *A* and *D*). 8-Br-cAMP is also known to stimulate $I_{Ca,L}$ through activation of the high voltage $Ca_V1.2$ channels in ventricular myocytes at a much higher concentration (1 (45) and 2 mM (46)). To eliminate the possible involvement of $I_{Ca,L}$ in the 8-Br-cAMP-induced I_{Ca} response, the cells were perfused with 10 μM nitrendipine, a specific blocker of the $I_{Ca,L}$. Perfusion with 10 μM nitrendipine did not affect the peak $I_{Ca,T}$. However,

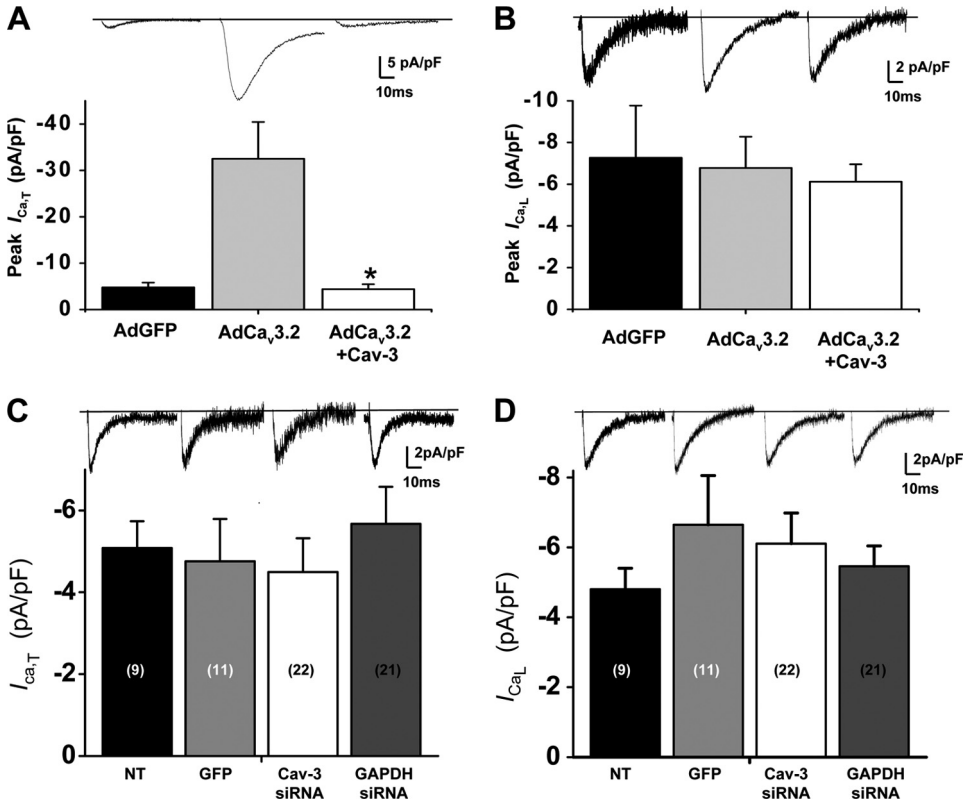

FIGURE 6. **Cav-3 inhibits $I_{Cav3.2}$ in mouse neonatal ventricular myocytes.** *A*, average peak $I_{Ca,T}$ density in neonatal ventricular myocytes infected with AdGFP control or with either AdCa$_v$3.2 or AdCa$_v$3.2+Cav-3 as indicated in the *bar plot*. Cav-3 overexpression significantly inhibited the AdCa$_v$3.2-mediated increased $I_{Cav3.2}$. *B*, average densities of $I_{Ca,L}$ in neonatal ventricular myocytes infected with adenovirus as indicated. Adenovirus infection did not alter the average $I_{Ca,L}$ density in the cells. The data represent mean ± S.E. (n = 3–5 cells, *, $p > 0.005$ with respect to AdCa$_v$3.2). Whole cell patch clamp analysis on the effect of siRNA-mediated knockdown of Cav-3 on $I_{Ca,T}$ in mouse neonatal ventricular myocytes. *C*, average peak $I_{Ca,T}$ density from nontransfected control (*NT*), GFP control, siRNA to Cav-3 or siRNA to GAPDH (*control*)-transfected cells as indicated in the bar plot. Representative corresponding T-type current traces are shown *above*. *D*, average densities of $I_{Ca,L}$ in neonatal ventricular myocytes transfected as above and representative corresponding $I_{Ca,L}$ current traces are shown *above* the bar plot. The average peak $I_{Ca,T}$ or $I_{Ca,L}$ was not significantly different and the data represent mean ± S.E., number of cells used are indicated in *parentheses*.

upon perfusion with 0.5 mM NiCl, the $I_{Ca,T}$ was completely abolished, suggesting that 8-Br-cAMP stimulation of the I_{Ca} is specifically through activation of the T-type Ca^{2+} channel. To confirm that 8-Br-cAMP stimulation of the $I_{Ca,T}$ is dependent on PKA, we pretreated neonatal myocytes (8–12 h incubation) with the myristoylated PKA inhibitor peptide fragment 14-22 (10 μM). Pretreatment of cells with the specific PKA inhibitor peptide failed to evoke 8-Br-cAMP stimulation of the $I_{Ca,T}$ in the control siRNA-transfected myocytes, suggesting a PKA-dependent augmentation of $I_{Ca,T}$ by 8-Br-cAMP (Fig. 7, *C* and *D*). In the next set of experiments, we used myocytes that were transfected with siRNA to Cav-3. In contrast with the control siRNA-treated cells the siRNA-mediated Cav-3 knockdown almost completely abolished 8-Br-cAMP stimulation of the $I_{Ca,T}$ in the myocytes (Fig. 7, *B* and *D*). These findings confirm that Cav-3 is required for PKA-mediated regulation of the Ca$_v$3.2 T-type Ca^{2+} channels in the mouse neonatal ventricular myocytes.

DISCUSSION

In the present study we describe regulation of the Ca$_v$3.2 subunit of T-type Ca^{2+} channels by Cav-3 in the mouse ventricular myocytes. Double immunogold labeling and electron microscopy imaging data clearly demonstrate co-localization of the Ca$_v$3.2 channel with Cav-3 relative to caveolae in the mouse ventricular myocytes. Co-immunoprecipitation analysis suggested an association of Ca$_v$3.1 and Ca$_v$3.2 channel isoforms with Cav-3, the GST pulldown assay confirmed a close interaction between the Ca$_v$3.2 channel protein and Cav-3. Functional analysis using whole cell patch clamp in the heterologous expression system of HEK293 cells demonstrated Cav-3 inhibition of the Ca$_v$3.2 channel but not Ca$_v$3.1 channel. In addition, we show that the N terminus region of Cav-3 interacts with the Ca$_v$3.2 channel and modulates the $I_{Cav3.2}$. Whole cell patch clamp studies using the neonatal cardiomyocytes demonstrated specific inhibition of $I_{Cav3.2}$ by Cav-3. On the other hand, siRNA-mediated knockdown of Cav-3 eliminated PKA regulation of the $I_{Ca,T}$.

T-type Ca^{2+} channels are known to modulate Ca^{2+} influx, membrane potential and hormone secretion. Of the three different T-type Ca^{2+} channel isoforms reported, alternative splicing of the Ca$_v$3.2 channels results in functional diversity of the channel during cardiac development (47). Recent findings using a heterologous expression system of HEK293 cells suggest a complex regulation for the Ca$_v$3.2 channels. It is well known that G-protein-dependent signaling pathways modulate native T-type Ca^{2+} channels (2). Extensive studies

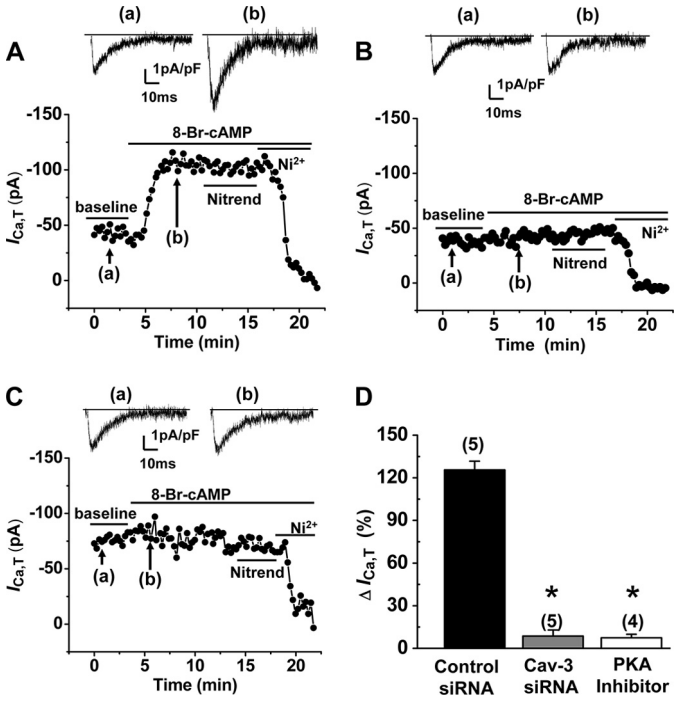

FIGURE 7. **siRNA-mediated knockdown of Cav-3 expression eliminated PKA-mediated 8-Br-cAMP stimulation of $I_{Ca,T}$ in neonatal mouse ventricular myocytes.** Perforated patch whole cell voltage clamp recordings of $I_{Ca,T}$ were performed by using a holding potential of −90 mV with 50-ms test pulses to −30 mV every 15 s in myocytes. *A*, peak $I_{Ca,T}$ is increased by stimulation with 8-Br-cAMP (100 μM) in a representative control siRNA-treated myocyte (whole cell capacitance = 8.6 picofarads); *B*, siRNA-mediated Cav-3 inhibition eliminated 8-Br-cAMP stimulation of $I_{Ca,T}$ in a representative myocyte (whole cell capacitance = 7.9 picofarads). *C*, pretreatment with 10 μM PKA inhibitor peptide completely inhibited the 8-Br-cAMP stimulation of the $I_{Ca,T}$ in a representative control siRNA-treated myocyte (whole cell capacitance = 11.9 picofarads). In all the groups of cells, perfusion with 10 μM nitrendipine (*Nitrend*) did not block I_{Ca}, whereas 0.5 mM Ni^{2+} completely inhibited I_{Ca}, indicating a stimulation of the T-type Ca^{2+} current by 8-Br-cAMP. *D*, average effect of 8-Br-cAMP stimulation on $I_{Ca,T}$ in myocytes with and without Cav-3 siRNA inhibition. The data represent mean ± S.E., number of cells used is indicated in *parentheses* *, $p <$ 0.001 relative to control.

from the laboratory of P. Berrett have demonstrated $Ca_v3.2$ channel regulation by PKA (48), Ca^{2+}/calmodulin-dependent protein kinase II (49, 50), and inhibition by G$\beta\gamma$ (51, 52). Another study demonstrated a selective inhibition of the $Ca_v3.2$ channel by corticotropin releasing factor receptor-1 is likely mediated by $\beta\gamma$ (53). On the other hand, a recent study demonstrated phospholipase Cβ, and protein kinase C modulation of the $Ca_v3.2$ channel mediated by $G_{q/11}$ in a voltage and G$\beta\gamma$ independent fashion (54). In addition in DRG neurons, monocyte chemoattractant protein-1 (a cytokine) was shown to inhibit $Ca_v3.2$ channels (55). The present work demonstrates that Cav-3 modulates transiently expressed $Ca_v3.2$ in HEK293 cells and native $Ca_v3.2$ current in neonatal mouse cardiomyocytes. Co-expression of Cav-3 inhibited $I_{Cav3.2}$ without altering the biophysical properties of the $Ca_v3.2$ channel, suggesting that Cav-3 modulates $Ca_v3.2$ current possibly in a voltage independent fashion. Our surface biotinylation data demonstrate that Cav-3 co-expression did not alter plasma membrane expression of the $Ca_v3.2$ channels, which rules out the possibility of internalization of the $Ca_v3.2$ channels. Thus, Cav-3 inhibition of $I_{Cav3.2}$ could possibly result through different signaling molecules associated with Cav-3.

Although it is clear from our GST-Cav-3 pulldown experiments that the N terminus region of Cav-3 interacts with the $Ca_v3.2$ channel and modulates the $I_{Cav3.2}$, there exists a likely possibility of direct interaction between the $Ca_v3.2$ channel and Cav-3. The intracellular linker region between domains II and III for the $Ca_v3.2$ channel contains clusters of serine and threonine residues and has been identified as an important region for interaction and regulation of the channel by serine/threonine kinases and G-protein signaling pathway proteins (3). In this context, it may not be unreasonable to hypothesize an interaction between the N terminus region of Cav-3 and the intracellular loop between domains II and III of the $Ca_v3.2$ channel. Further studies are needed to identify the site of $Ca_v3.2$ channel involved in the interaction with Cav-3, which may also help us understand dynamic regulation of the $Ca_v3.2$ channels.

We observed that siRNA-mediated knockdown of Cav-3 did not affect the $I_{Ca,T}$ density in the mouse neonatal cardiomyocytes but abolished PKA regulation of the $I_{Ca,T}$. Similar to this observation, in an earlier study we had demonstrated that a subpopulation of the $Ca_v1.2$ L-type Ca^{2+} channels are localized to caveolae and siRNA-mediated Cav-3 knockdown did not affect the $I_{Ca,L}$ density in neonatal ventricular myocytes. However, Cav-3 knockdown specifically inhibited the β_2-adrenergic receptor regulation of the $Ca_v1.2$ channels (24). Caveolins contain scaffolding domains that interact with multiple signaling molecules including G-proteins and coupled receptors, regulatory proteins such as Ca^{2+}/calmodulin-dependent protein kinase II, PKA, and PKC, and some ion channels, thereby providing temporal and spatial regulation of cellular signal transduction (18, 56, 57). The subcellular localization of ion channels to caveolae allows the integration of these channels into specific macromolecular signaling complexes in a distinct lipid microenvironment providing for their precise modulation. Caveolar localization and Cav-3 inhibition of $Ca_v3.2$ channels in neonatal cardiomyocytes explains the compartmentalized and dynamic regulation of the $Ca_v3.2$ channels by PKA and possibly other kinases in the native cells. Perhaps, caveolar localization and Cav-3 interaction of the $Ca_v3.2$ are necessary for precise modulation of this channel not only by PKA but also by different signaling molecules during normal and pathological states.

Expression of Cav-3 is developmentally regulated as it increases postnatally and reaches maximum levels by days 4–5 followed by a decrease to stable expression levels seen in the adult cardiomyocytes (58, 59). The cardiac T-type Ca^{2+} channels are abundantly expressed during cardiac development but their expression is not detected in normal adult ventricular myocytes. It is well established that moderate to severe ventricular tissue remodeling occurs, with associated changes at the single myocyte level, during pathological states such as cardiac hypertrophy and heart failure (60–62). During cardiac hypertrophy, $Ca_v3.1$ and $Ca_v3.2$ channels are known to be up-regulated in the ventricular myocytes. Caveolae and expression of Cav-3 is also known to be altered during these conditions (63, 64). It may also be possible that during the ventricular remodeling process altered Cav-3 and caveolae expression could alter subcellular localization and expression

of the Ca^{2+} channels, including the $Ca_v3.2$ channels that may result in altered coupling and regulation of the channels. The $Ca_v3.2$ T-type Ca^{2+} channels are involved in various diseases such as epilepsy (39, 65–67), pain (68), hypertension (69), and cardiac hypertrophy (16). In fact, using genetic deletion of *CACNA1H*, which encodes the Cav3.2 channel, it was demonstrated that the $Ca_v3.2$ T-type Ca^{2+} channel is required for induction of pathological cardiac hypertrophy (16). One other report indicated that overexpression of Cav-3 is protective against agonist-induced hypertrophic responses in the rat neonatal cardiomyocytes (70). In our studies overexpression of Cav-3 specifically inhibited the T-type Ca^{2+} current without affecting the L-type Ca^{2+} currents, which are also known to localize to caveolae and associate with Cav-3 (24). Our data also demonstrate that Cav-3 specifically inhibited the adenovirus-mediated increased overexpression of $I_{Cav3.2}$. In this context our finding may have important therapeutic implications pertaining to the T-type Ca^{2+} channel block, because, T-type Ca^{2+} channel blockers have been proposed to be useful in the therapeutics of a variety of conditions including hypertension and heart failure (69, 71). Further studies are needed to understand the role of Cav-3 and caveolae in the ventricular remodeling process during cardiac disease conditions such as hypertrophy and heart failure. Regulation of the T-type Ca^{2+} channels and Ca^{2+} signaling by caveolae is important for understanding the mechanism of pathological changes in cardiac hypertrophy and heart failure.

In summary, our results demonstrate for the first time a precise caveolar localization of the $Ca_v3.2$ T-type Ca^{2+} channel in cardiomyocytes. We show that Cav-3 interacts with the $Ca_v3.2$ channels and modulates PKA regulation of $I_{Ca,T}$ in the ventricular myocytes. Our studies provide the basis for understanding the compartmentalized regulation of the T-type Ca^{2+} channel in cardiomyocytes and other cell types in normal and pathological conditions.

Acknowledgments—We are grateful to Benjamin August (University Of Wisconsin School of Medicine Electron Microscope Facility). We are grateful to Thankful Sanftleben for assistance with manuscript preparation.

REFERENCES

1. Perez-Reyes, E. (2003) *Physiol. Rev.* **83,** 117–161
2. Iftinca, M. C., and Zamponi, G. W. (2009) *Trends Pharmacol. Sci.* **30,** 32–40
3. Huc, S., Monteil, A., Bidaud, I., Barbara, G., Chemin, J., and Lory, P. (2009) *Biochim. Biophys. Acta* **1793,** 947–952
4. Lee, J. H., Daud, A. N., Cribbs, L. L., Lacerda, A. E., Pereverzev, A., Klöckner, U., Schneider, T., and Perez-Reyes, E. (1999) *J. Neurosci.* **19,** 1912–1921
5. Klöckner, U., Lee, J. H., Cribbs, L. L., Daud, A., Hescheler, J., Pereverzev, A., Perez-Reyes, E., and Schneider, T. (1999) *Eur. J. Neurosci.* **11,** 4171–4178
6. Kozlov, A. S., McKenna, F., Lee, J. H., Cribbs, L. L., Perez-Reyes, E., Feltz, A., and Lambert, R. C. (1999) *Eur. J. Neurosci.* **11,** 4149–4158
7. Chemin, J., Monteil, A., Perez-Reyes, E., Bourinet, E., Nargeot, J., and Lory, P. (2002) *J. Physiol.* **540,** 3–14
8. McGivern, J. G. (2006) *Drug Discov. Today* **11,** 245–253
9. Vassort, G., Talavera, K., and Alvarez, J. L. (2006) *Cell Calcium* **40,** 205–220
10. Ono, K., and Iijima, T. (2010) *J. Mol. Cell Cardiol.* **48,** 65–70
11. Nuss, H. B., and Marban, E. (1994) *J. Physiol.* **479,** 265–279
12. Cribbs, L. L., Martin, B. L., Schroder, E. A., Keller, B. B., Delisle, B. P., and Satin, J. (2001) *Circ. Res.* **88,** 403–407
13. Nuss, H. B., and Houser, S. R. (1993) *Circ. Res.* **73,** 777–782
14. Martínez, M. L., Heredia, M. P., and Delgado, C. (1999) *J. Mol. Cell Cardiol.* **31,** 1617–1625
15. Ferron, L., Capuano, V., Ruchon, Y., Deroubaix, E., Coulombe, A., and Renaud, J. F. (2003) *Circ. Res.* **93,** 1241–1248
16. Chiang, C. S., Huang, C. H., Chieng, H., Chang, Y. T., Chang, D., Chen, J. J., Chen, Y. C., Chen, Y. H., Shin, H. S., Campbell, K. P., and Chen, C. C. (2009) *Circ. Res.* **104,** 522–530
17. Insel, P. A., and Patel, H. H. (2009) *Curr. Opin. Nephrol. Hypertens.* **18,** 50–56
18. Balijepalli, R. C., and Kamp, T. J. (2008) *Prog. Biophys. Mol. Biol.* **98,** 149–160
19. Pani, B., and Singh, B. B. (2009) *Cell Calcium* **45,** 625–633
20. Glenney, J. R., Jr. (1992) *FEBS Lett.* **314,** 45–48
21. Scherer, P. E., Okamoto, T., Chun, M., Nishimoto, I., Lodish, H. F., and Lisanti, M. P. (1996) *Proc. Natl. Acad. Sci. U.S.A.* **93,** 131–135
22. Song, K. S., Scherer, P. E., Tang, Z., Okamoto, T., Li, S., Chafel, M., Chu, C., Kohtz, D. S., and Lisanti, M. P. (1996) *J. Biol. Chem.* **271,** 15160–15165
23. Boulware, M. I., Kordasiewicz, H., and Mermelstein, P. G. (2007) *J. Neurosci.* **27,** 9941–9950
24. Balijepalli, R. C., Foell, J. D., Hall, D. D., Hell, J. W., and Kamp, T. J. (2006) *Proc. Natl. Acad. Sci. U.S.A.* **103,** 7500–7505
25. Yarbrough, T. L., Lu, T., Lee, H. C., and Shibata, E. F. (2002) *Circ. Res.* **90,** 443–449
26. Ye, B., Balijepalli, R. C., Foell, J. D., Kroboth, S., Ye, Q., Luo, Y. H., and Shi, N. Q. (2008) *Biochemistry* **47,** 12312–12318
27. Bossuyt, J., Taylor, B. E., James-Kracke, M., and Hale, C. C. (2002) *Ann. N.Y. Acad. Sci.* **976,** 197–204
28. Cribbs, L. L., Gomora, J. C., Daud, A. N., Lee, J. H., and Perez-Reyes, E. (2000) *FEBS Lett.* **466,** 54–58
29. Balijepalli, R. C., Delisle, B. P., Balijepalli, S. Y., Foell, J. D., Slind, J. K., Kamp, T. J., and January, C. T. (2007) *Channels* **1,** 263–272
30. Wagoner, L. E., Zhao, L., Bishop, D. K., Chan, S., Xu, S., and Barry, W. H. (1996) *Circulation* **93,** 111–119
31. Yao, Q., Chen, J., Cao, H., Orth, J. D., McCaffery, J. M., Stan, R. V., and McNiven, M. A. (2005) *J. Mol. Biol.* **348,** 491–501
32. Rothberg, K. G., Heuser, J. E., Donzell, W. C., Ying, Y. S., Glenney, J. R., and Anderson, R. G. (1992) *Cell* **68,** 673–682
33. Cohen, R. M., Foell, J. D., Balijepalli, R. C., Shah, V., Hell, J. W., and Kamp, T. J. (2005) *Am. J. Physiol. Heart Circ. Physiol.* **288,** H2363–H2374
34. Brueggemann, L. I., Martin, B. L., Barakat, J., Byron, K. L., and Cribbs, L. L. (2005) *Am. J. Physiol. Heart Circ. Physiol.* **288,** H923–H935
35. Rockman, H. A., Ross, R. S., Harris, A. N., Knowlton, K. U., Steinhelper, M. E., Field, L. J., Ross, J., Jr., and Chien, K. R. (1991) *Proc. Natl. Acad. Sci. U.S.A.* **88,** 8277–8281
36. Martin, R. L., Lee, J. H., Cribbs, L. L., Perez-Reyes, E., and Hanck, D. A. (2000) *J. Pharmacol. Exp. Ther.* **295,** 302–308
37. Talavera, K., Staes, M., Janssens, A., Klugbauer, N., Droogmans, G., Hofmann, F., and Nilius, B. (2001) *J. Biol. Chem.* **276,** 45628–45635
38. Foell, J. D., Balijepalli, R. C., Delisle, B. P., Yunker, A. M., Robia, S. L., Walker, J. W., McEnery, M. W., January, C. T., and Kamp, T. J. (2004) *Physiol. Genomics* **17,** 183–200
39. Khosravani, H., Altier, C., Simms, B., Hamming, K. S., Snutch, T. P., Mezeyova, J., McRory, J. E., and Zamponi, G. W. (2004) *J. Biol. Chem.* **279,** 9681–9684
40. Ono, K., and Iijima, T. (2005) *J. Pharmacol. Sci.* **99,** 197–204
41. Lee, J. H., Gomora, J. C., Cribbs, L. L., and Perez-Reyes, E. (1999) *Biophys. J.* **77,** 3034–3042
42. Alvarez, J. L., and Vassort, G. (1992) *J. Gen. Physiol.* **100,** 519–545
43. Lenglet, S., Louiset, E., Delarue, C., Vaudry, H., and Contesse, V. (2002) *Endocrinology* **143,** 1748–1760
44. Kim, J. A., Park, J. Y., Kang, H. W., Huh, S. U., Jeong, S. W., and Lee,

J. H. (2006) *J. Pharmacol. Exp. Ther.* **318,** 230–237
45. Beetz, N., Hein, L., Meszaros, J., Gilsbach, R., Barreto, F., Meissner, M., Hoppe, U. C., Schwartz, A., Herzig, S., and Matthes, J. (2009) *Cardiovasc. Res.* **84,** 396–406
46. Xiao, L., Yuan, X., and Sharkis, S. J. (2006) *Stem Cells* **24,** 1476–1486
47. David, L. S., Garcia, E., Cain, S. M., Thau, E. M., Tyson, J. R., and Snutch, T. P. (2010) *Channels* **4,** 375–389
48. Hu, C., Depuy, S. D., Yao, J., McIntire, W. E., and Barrett, P. Q. (2009) *J. Biol. Chem.* **284,** 7465–7473
49. Wolfe, J. T., Wang, H., Perez-Reyes, E., and Barrett, P. Q. (2002) *J. Physiol.* **538,** 343–355
50. Welsby, P. J., Wang, H., Wolfe, J. T., Colbran, R. J., Johnson, M. L., and Barrett, P. Q. (2003) *J. Neurosci.* **23,** 10116–10121
51. Wolfe, J. T., Wang, H., Howard, J., Garrison, J. C., and Barrett, P. Q. (2003) *Nature* **424,** 209–213
52. DePuy, S. D., Yao, J., Hu, C., McIntire, W., Bidaud, I., Lory, P., Rastinejad, F., Gonzalez, C., Garrison, J. C., and Barrett, P. Q. (2006) *Proc. Natl. Acad. Sci. U.S.A.* **103,** 14590–14595
53. Tao, J., Hildebrand, M. E., Liao, P., Liang, M. C., Tan, G., Li, S., Snutch, T. P., and Soong, T. W. (2008) *Mol. Pharmacol.* **73,** 1596–1609
54. Rangel, A., Sánchez-Armass, S., and Meza, U. (2010) *Mol. Pharmacol.* **77,** 202–210
55. You, H., Altier, C., and Zamponi, G. W. (2010) *Mol. Pharmacol.* **77,** 211–217
56. Steinberg, S. F. (2004) *J. Mol. Cell Cardiol.* **37,** 407–415
57. Patel, H. H., Murray, F., and Insel, P. A. (2008) *Handb. Exp. Pharmacol.* **185,** 167–184
58. Ostadal, B., Ostadalova, I., and Dhalla, N. S. (1999) *Physiol. Rev.* **79,** 635–659
59. Ratajczak, P., Oliviéro, P., Marotte, F., Kolar, F., Ostadal, B., and Samuel, J. L. (2005) *J. Appl. Physiol.* **99,** 244–251
60. Balijepalli, R. C., Lokuta, A. J., Maertz, N. A., Buck, J. M., Haworth, R. A., Valdivia, H. H., and Kamp, T. J. (2003) *Cardiovasc. Res.* **59,** 67–77
61. Lyon, A. R., MacLeod, K. T., Zhang, Y., Garcia, E., Kanda, G. K., Lab, M. J., Korchev, Y. E., Harding, S. E., and Gorelik, J. (2009) *Proc. Natl. Acad. Sci. U.S.A.* **106,** 6854–6859
62. Wei, S., Guo, A., Chen, B., Kutschke, W., Xie, Y. P., Zimmerman, K., Weiss, R. M., Anderson, M. E., Cheng, H., and Song, L. S. (2010) *Circ. Res.* **107,** 520–531
63. Hare, J. M., Lofthouse, R. A., Juang, G. J., Colman, L., Ricker, K. M., Kim, B., Senzaki, H., Cao, S., Tunin, R. S., and Kass, D. A. (2000) *Circ. Res.* **86,** 1085–1092
64. Kikuchi, T., Oka, N., Koga, A., Miyazaki, H., Ohmura, H., and Imaizumi, T. (2005) *J. Cardiovasc. Pharmacol.* **45,** 204–210
65. Khosravani, H., Bladen, C., Parker, D. B., Snutch, T. P., McRory, J. E., and Zamponi, G. W. (2005) *Ann. Neurol.* **57,** 745–749
66. Becker, A. J., Pitsch, J., Sochivko, D., Opitz, T., Staniek, M., Chen, C. C., Campbell, K. P., Schoch, S., Yaari, Y., and Beck, H. (2008) *J. Neurosci.* **28,** 13341–13353
67. Powell, K. L., Cain, S. M., Ng, C., Sirdesai, S., David, L. S., Kyi, M., Garcia, E., Tyson, J. R., Reid, C. A., Bahlo, M., Foote, S. J., Snutch, T. P., and O'Brien, T. J. (2009) *J. Neurosci.* **29,** 371–380
68. Maeda, Y., Aoki, Y., Sekiguchi, F., Matsunami, M., Takahashi, T., Nishikawa, H., and Kawabata, A. (2009) *Pain* **142,** 127–132
69. Ball, C. J., Wilson, D. P., Turner, S. P., Saint, D. A., and Beltrame, J. F. (2009) *Hypertension* **53,** 654–660
70. Koga, A., Oka, N., Kikuchi, T., Miyazaki, H., Kato, S., and Imaizumi, T. (2003) *Hypertension* **42,** 213–219
71. Kinoshita, H., Kuwahara, K., Takano, M., Arai, Y., Kuwabara, Y., Yasuno, S., Nakagawa, Y., Nakanishi, M., Harada, M., Fujiwara, M., Murakami, M., Ueshima, K., and Nakao, K. (2009) *Circulation* **120,** 743–752